

Lifshitz transitions and elastic properties of Osmium under pressure

Daniela Koudela, Manuel Richter, Arnulf Möbius, Klaus Koepernik, and Helmut Eschrig
IFW Dresden, PF 270 116, D-01171 Dresden, Germany

(Dated: July 30, 2018)

Topological changes of the Fermi surface under pressure may cause anomalies in the low-temperature elastic properties. Our density functional calculations for elemental Osmium evidence that this metal undergoes three such Lifshitz transitions in the pressure range between 70 GPa and 130 GPa. The related elastic anomalies are, however, invisibly weak. The critical pressures considerably exceed the values for recently measured and calculated anomalies in the pressure (P) dependence of the hexagonal c/a lattice parameter ratio close to 25 GPa. We demonstrate that the latter anomalies are statistically not significant and that $(c/a)(P)$ can be fitted equally well by a smooth dependence.

PACS numbers: 71.18.+y, 71.15.Nc, 64.30.+t

I. INTRODUCTION

Since Lifshitz' seminal publication,¹ the search for electronic topological transitions (ETT) of the Fermi surface (FS) has been a subject of permanent interest, for reviews see Refs. 2 and 3. As a true phase transition it may appear only at $T = 0$ in highly pure samples, otherwise it is just a crossover. While alloying may change the band filling and, thus, the number or connectivity of the FS sheets, it unavoidably smears the electron states and the observable effects. Magnetic field can cause ETT as well,⁴ but the field strength required to achieve a Lifshitz transition in a conventional metal is beyond the present technical possibilities. Thus, low-temperature pressure experiments are most promising to find measurable effects related to ETT.²

All thermodynamic and transport properties of a metal are influenced by the topology of the FS to some extent. In the past, transport properties were in the focus of research, since the impact of ETT on the transport is stronger than on, e.g., elastic properties.³ As an example, Godwal *et al.*⁵ found a Lifshitz transition in AuIn₂, where measurements yield anomalies in the electrical resistivity and in the thermoelectric power in the 2 – 4 GPa pressure range, but angle-dispersive x-ray-diffraction measurements do not indicate any structural anomaly. Very recently, an elastic anomaly was observed in YCo₅ under pressure, caused by an exceptionally strong van Hove singularity in the electronic density of states (DOS).⁶

The question whether Lifshitz transitions are visible in the c/a ratio of the hexagonal lattice parameters of Zinc or if their effect is below the limit of detectability is controversially discussed in the literature. Earlier experimental evidence⁷ for an anomaly was later traced back to non-hydrostatic pressure conditions,⁸ and earlier theoretical confirmations of the elastic anomaly were found to be caused by insufficient \mathbf{k} -point sampling.⁹ This discussion has recently been resumed¹⁰ by an alternative presentation of the hydrostatic pressure data from Ref. 8.

A similar puzzling situation is present in the case of the 5d element Osmium, which is one of the densest elements

and the metal with the largest bulk modulus. Occelli *et al.* measured the lattice parameters of Os under pressure, found a discontinuity in the first pressure derivative of the c/a ratio at about 25 GPa, and assigned this anomaly to a Lifshitz transition.¹¹ On the other hand, Takemura did not infer an anomaly from his related data obtained by similar measurements.¹² Subsequently, two theoretical papers were published confirming the existence of an anomaly in c/a versus pressure at about 10 GPa¹³ and at 27 GPa,¹⁴ respectively. However, no reason for this anomaly was disclosed in the electronic structure. In particular, the FS topology was found unchanged up to a pressure of 80 GPa.¹⁴

As an attempt to get a more detailed understanding of the dependence of the c/a ratio of Osmium under pressure, we have carried out very precise density functional calculations applying the FPLO code,¹⁵ considering pressures up to 180 GPa. We identified three ETT in the high pressure region. Further, we confirm the finding of Ma and co-workers¹⁴ that there is no ETT within the parameter range they considered. Our calculations yield pressure dependent lattice parameters that are in accord with those presented by the previous authors. Statistical analysis of both our and previously published data eventually shows that there is no reason to assume a discernible anomaly in the dependence of c/a on pressure from ETT.

II. DETAILS OF CALCULATION

Calculations were performed for the hexagonal close-packed structure (hcp, P6₃/mmc, space group 194) which is the equilibrium structure of Osmium in the considered pressure range.¹⁶ The four-component relativistic version of the full potential local orbital (FPLO) band structure code,¹⁵ release 5, was used. It accounts for kinematic relativistic effects including spin-orbit coupling to all orders. In the case of Osmium, the $d_{3/2}$ - $d_{5/2}$ splitting is 1 eV. Therefore it cannot be neglected in the present analysis. After test calculations with different basis sets we decided to use a minimum basis consisting of $4f5s5p$ states

in the semicore and $6s6p5d$ states in the valence. All lower lying states were treated as core states. A \mathbf{k} -mesh subdivision of $48 \times 48 \times 48$ \mathbf{k} -points in the full Brillouin zone (BZ) was used, which corresponds to 5425 \mathbf{k} -points in the irreducible part of BZ. This mesh is significantly finer than the meshes used by Ma *et al.*, $16 \times 16 \times 12$ in the BZ,¹⁴ and by Sahu and Kleinman, 84 points¹³ in the irreducible part of BZ. For calculating the density of states, the \mathbf{k} -mesh was refined to $96 \times 96 \times 96$ \mathbf{k} -points in the full BZ (40033 \mathbf{k} -points in the irreducible BZ). The \mathbf{k} -space integrations were carried out with the linear tetrahedron method.¹⁷ For the exchange-correlation potential we employed the local density approximation (LDA) in the version proposed by Perdew and Wang, 1992.¹⁸

III. TOTAL ENERGY CALCULATIONS

The upper panel of Figure 1 shows the total energy of Osmium plotted against volume V , where the c/a ratio has been relaxed for each volume, $E_{\text{total}}(V) = \min_{(c/a)} E_{\text{total}}(V, c/a)$, which is the correct condition for hydrostatic pressure. The red (gray) dashed line shows the experimental volume (taken from Ref. 11), determined in a room-temperature experiment. The calculated equilibrium volume is 0.3% smaller than the measured room-temperature volume. Accounting for thermal expansion provides an almost perfect agreement. It is a known but not yet understood feature of LDA, that it reproduces the ground state volumes of the heavy 5d elements much better than gradient approximations.¹⁹ We take the agreement in the present case as justification to rely on LDA in the further investigations.

The inset of Figure 1, upper panel, proves the exceptional stability of the calculations. Each data point in the figure is taken from independent self-consistency runs and independent c/a optimizations. The FPLO code¹⁵ yields a very smooth energy-curve, with numerical noise well below the $\mu\text{Hartree}$ range. We took advantage of this stability in the evaluation of the equation of state (EOS) and the pressure dependence of c/a , presented in Section VI: While the calculations yield directly the two dependences $E_{\text{total}}(V)$ and $(c/a)(V)$, in experiment the pressure $P = -(dE_{\text{total}}/dV)$ may be measured independently. Instead of relying on an analytic fit of Birch-Murnaghan type for $E_{\text{total}}(V)$ we calculated the derivative numerically by means of the three-point formula, $f'((x_1 + x_2)/2) \approx (f(x_2) - f(x_1))/(x_2 - x_1)$, considering neighboring V values. This seemingly less sophisticated procedure solves a dilemma, which is present for analytic fits. If an analytic fit is used for the whole volume range considered, the anomaly will be removed by the fit. If the analytic fit is done piece-wise, anomalies will necessarily be produced at the end points of the respective fit regions, due to different noise in the adjacent regions. Previous authors used one fit for the whole range.^{13,14} We checked our procedure by comparing the evaluated pressures with

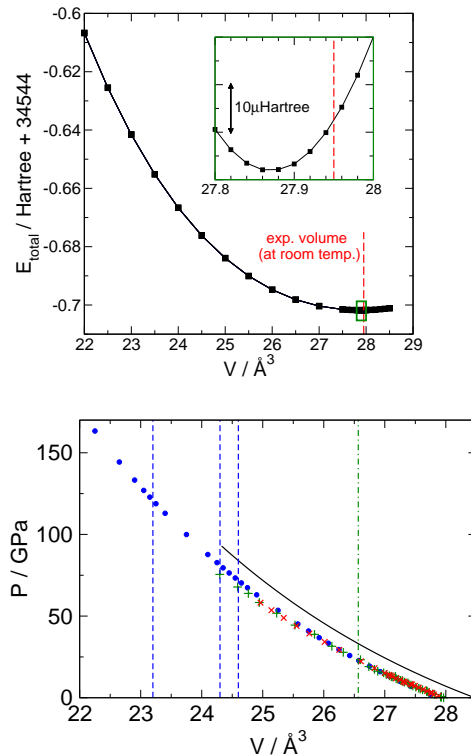


FIG. 1: (color online). Upper panel: total energy versus unit cell volume with relaxed c/a ratio. The red (gray) dashed line marks the experimental room-temperature volume. Inset: magnification of the total energy versus volume curve around the minimum. In the large graph this region is marked with a green (gray) box. Lower panel: equation of state of Osmium. Blue (black) circles: present calculations; green (gray) pluses and red (gray) crosses: experimental data from Ocelli *et al.*¹¹ and from Takemura,¹² respectively; black line: calculations by Ma *et al.*¹⁴. The green (gray) dashed-dotted line denotes the volume where Ocelli *et al.*¹¹ find an elastic anomaly. The blue (black) dashed lines indicate the volumes where Lifshitz transitions are found in the present calculations.

five different fits of Birch-Murnaghan type. For 80% of the pressure range between zero and 180 GPa, our numerical fit lies within the $P(V)$ values spanned by the different analytic fits. The maximum difference between any of the analytic fits and the numerical fit amounts to 0.2 GPa, and the mean difference amounts to 0.1 GPa.

Figure 1, lower panel, shows the EOS of Osmium. Green (gray) pluses and red (gray) crosses denote experimental data by Ocelli *et al.*¹¹ and by Takemura,¹² respectively. Both data sets do not deviate from each other on the scale of this figure. The blue (black) circles denote results of the present calculations, obtained from the $E(V)$ data, upper panel of Figure 1, by numerical differentiation. The EOS calculated using LDA coincides with the experimental data in the low-pressure range up to about 40 GPa. It slightly over-estimates the pressure in the higher-pressure range.

Results from calculations by Ma *et al.*¹⁴ are depicted by a black line. These calculations were carried out in the GGA which systematically over-estimates the zero-pressure volume of heavy 5d metals.¹⁹ Accordingly, the GGA data run almost parallel to the LDA data, with a volume offset of about 2%. An alternative presentation, $P(V/V_0)$ with $V_0 = V(P = 0)$, yields a very good coincidence of both calculated data sets. As stated before, the offset explains the fact that Ma *et al.* did not find any ETT in their calculations up to 80 GPa,¹⁴ while we find the first ETT at about 72 GPa.

In the lower panel of Fig. 1, there is no anomaly of the EOS visible in any data set at any pressure, in agreement with the earlier presentations of the quoted data and with the weakness of the Lifshitz transitions disclosed in this paper.

IV. THE FERMI SURFACE UNDER PRESSURE

It was suggested by Occelli *et al.*, that the observed anomaly in $(c/a)(P)$ should arise from an ETT. Thus, we first investigate the volume dependence of the FS in the range $22.0 \text{ \AA}^3 \leq V \leq 28.0 \text{ \AA}^3$. This volume dependence translates into a pressure dependence through the EOS given in the lower panel of Figure 1, $P \lesssim 180 \text{ GPa}$. As in the evaluation of the total energy, c/a has been relaxed for each volume.

At zero pressure, the FS of Osmium has four sheets, see Figure 2. The first sheet consists of small hole ellipsoids located at the line L-M. Occelli *et al.* suspected these ellipsoids to disappear under pressure.¹¹ The second sheet is a big monster surface, which is closed in z-direction (compare Figure 3) but connected in the x-y plane. The third and fourth sheets are closed surfaces, which are nested and centered around the Γ -point. The inner one of the two is waisted. Our calculated zero-pressure FS agrees well with measurements of Kamm and Anderson,²⁰ with the calculated FS of Smelyansky *et al.*,²¹ and with the more recent calculation of Ma *et al.*¹⁴

Figure 3 shows a comparison of the FS at zero pressure (first row, $V = 27.87 \text{ \AA}^3$, $c/a = 1.5850$) with the FS calculated at a very high pressure of about 180 GPa (second row, $V = 22.0 \text{ \AA}^3$, $c/a = 1.5968$). It is obvious, that the small hole ellipsoid between L and M does not disappear under pressure. On the contrary, it grows. Nevertheless, we find a Lifshitz transition in the first FS sheet: a further tiny hole ellipsoid appears under pressure at the L-point. Another Lifshitz transition takes place in the second FS. Here, a neck is created under pressure, centered at L. The third FS sheet is not displayed in Figure 3 because its topology is preserved in the considered pressure range. Finally, a third ETT is found inside the fourth FS sheet, where a hole ellipsoid appears under pressure at the Γ -point.

At which pressure/volume the FS changes its topology depends on the c/a ratio. This can be seen in Figure 4.

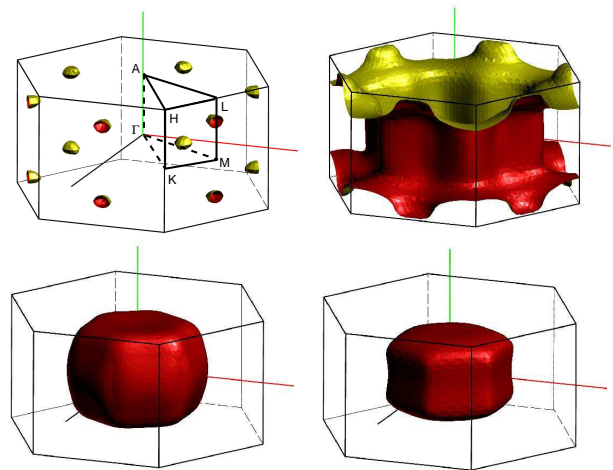


FIG. 2: (color online). The Fermi surface of Osmium at zero pressure. First, second, third, and fourth sheets are given separately in the upper left, upper right, lower left, and lower right panel, respectively. Red (black) and yellow (light-gray) colors denote occupied and unoccupied sides of the Fermi surface, respectively.

Reducing the volume under hydrostatic pressure, starting at the zero-pressure value, one finds the following sequence of transitions: At first, the additional ellipsoid at the Γ -point appears at $V = 24.60 \text{ \AA}^3$, then the neck is formed at $V = 24.20 \text{ \AA}^3$, and finally the additional ellipsoid at the L-point appears at $V = 23.20 \text{ \AA}^3$. The related transition pressures are 72 GPa, 81 GPa, and 122 GPa. Worth mentioning, a peculiarity relates the latter two ETT. Namely, two necks are formed at first at the mentioned volume which are situated at the line L-H. These necks merge at L at the same pressure that lets the L-point ellipsoid appear. This coincidence is due to a degeneracy of the first and second sheet bands along L-A, see Figure 5.

If we presume the experimentally measured and extrapolated $(c/a)(V)$, the ETT take place at pressures of about 50 GPa (ellipsoid at the Γ -point), at about 87 GPa (neck at the line L-H) and at about 122 GPa (ellipsoid at the L-point).

The discussed topological changes can be clearly identified in the band structure plots. For each hole ellipsoid appearing under pressure one expects a related maximum in the band dispersion to cross the Fermi energy. In the case of the neck, a saddle-point of band dispersion should cross the Fermi level. This saddle-point does not lie on a symmetry-point but only on a symmetry-line of the Brillouin zone and thus appears only as a maximum in the band structure plot.

Figure 5 shows the band structure for zero pressure (upper panel) and under a high hydrostatic pressure of about 180 GPa (lower panel). The loci of the three discussed ETT are marked by red (gray) full-line circles. The pressure-induced Fermi level crossing of all these three band maxima is obvious. The blue (black) dashed-

line circles in Figure 5 mark the place of the disappearance of a hole pocket proposed in Ref. 11. The related maximum does, however, not fall below the Fermi level under pressure but gets shifted to higher energy instead.

Summarizing this section, we find three distinct Lifshitz transitions in the pressure range between 70 GPa and 130 GPa. In the range of 25 GPa the present calculations do not yield an anomaly of c/a caused by the electronic structure. None of the transitions disclosed here were found in the earlier calculations restricted to a pressure range just below the first observed transition.¹⁴ Note, that the Fermi surface topology in the latter publication was investigated up to 80 GPa. The related *volume*, however, was slightly larger than our predicted first critical volume. The reason is that Ma *et al.* used the generalized gradient approximation (GGA), while we used LDA.

V. DENSITY OF STATES

ETT should manifest themselves in van Hove singularities of the DOS passing through the Fermi level under pressure. The upper panel of Figure 6 presents the DOS of Osmium at zero pressure and at about 180 GPa. The 5d band is considerably broadened at such a high pressure, in comparison with the zero pressure case. However, the Fermi level is situated in a smooth valley of the DOS in the whole pressure range. In particular, no Fermi level crossing of any singularity is obvious in this overview panel.

The lower part of Figure 6 shows the DOS close to the Fermi level in about hundredfold magnification, for five different pressures including the three transition pressures and the two limiting cases of the upper panel. A tiny anomaly, caused by the Lifshitz transitions, is found moving through the Fermi level. Despite the huge number of 96^3 \mathbf{k} -points in the full BZ used for these calculations, the estimated DOS resolution that can be achieved for the present band dispersions by means of the linear tetrahedron method amounts to 50 meV which is about the width of the observed anomaly. Thus, no details of this feature can be resolved, it remains unclear to which extent the individual ETT contribute to it. (Note, that the shape is changing with pressure. This fact also hints to resolution problems.)

As the ETT anomaly amounts to about 10^{-3} of the total DOS, it is probably impossible to detect it in the elastic properties. This becomes even more clear if we consider the volume dependence of the DOS at the Fermi energy, Figure 7, which decreases almost linearly with unit cell volume. The red (gray) solid line shows a linear fit to the data. No peculiarity is visible at the Lifshitz transitions, marked by blue (black) dashed lines. To understand this point, we have estimated the strength of the van Hove singularity related to the first ETT, the appearance of the ellipsoid at Γ . The extra contribution

to the DOS due to this ellipsoid can be calculated as

$$|\delta g(\varepsilon)| = \frac{V}{2\pi^2} \sqrt{\frac{8m_x m_y m_z}{\hbar^6}} \sqrt{(\varepsilon_{cr} - \varepsilon)} \quad (1)$$

with $V = 27.87 \text{ \AA}^3$. Here, $\hbar^2/2m_i$ denotes the curvature of the ellipsoid in direction i , which has been fitted to $\hbar^2/2m_x = 171.4 \text{ eV \AA}^2$, $\hbar^2/2m_y = 161.4 \text{ eV \AA}^2$ and $\hbar^2/2m_z = 97.1 \text{ eV \AA}^2$. Then $\delta g(\varepsilon) \approx 0.0009 \text{ eV}^{-1} \sqrt{(\varepsilon_{cr} - \varepsilon)/\text{eV}}$ or about 0.00009 eV^{-1} at 10 meV distance from the position of the van Hove singularity, ε_{cr} . Here, the crucial point is the tiny prefactor of the square-root singularity. This extra contribution to the pressure of the Fermi gas will not be visible in elastic data obtained by today's experimental or numerical means.

Summarizing this section, we find that the disclosed Lifshitz transitions are very weak and probably not detectable by measurements of elastic properties. However, there might be a chance of observing anomalies in magneto-transport or thermopower under pressure.

VI. c/a RATIO UNDER PRESSURE

We now proceed to a comparison of several measured and calculated variants of the pressure and volume dependence of the c/a ratio. A critical evaluation and data analysis will help to clarify the question, if there is any anomaly in the data close to 25 GPa (or 10 GPa), as proposed by several authors.^{11,13,14}

Figure 8 shows the dependence of c/a on volume and on pressure. Similar to the EOS case, both experimental data sets coincide within the error estimates given in Refs. 11 and 12. The three computed data sets run more or less parallel with the experimental ones. Unlike the EOS data, the offset of the LDA results of about 0.005 (blue (black) circles, present calculation, and violet (black) triangles, calculation by Sahu and Kleinman) is larger than the offset of the GGA results by Ma *et al.* (black diamonds). Additionally, we have introduced another data set (blue (black) open circles) in the lower panel of Figure 8, denoting our calculated data shifted down by 0.00515. These offset-corrected LDA data show a remarkable coincidence with the measured data both in slope and curvature. Thus, they can be used to extrapolate the experimental data into the high-pressure region in order to estimate experimental transition pressures given in Section IV.

In $(c/a)(V/V_0)$ no anomaly is visible at any of the Lifshitz transition volumes (blue (black) dashed lines), and no anomaly is visible either at a volume of about $0.95V_0$, corresponding to 25 GPa. The proposed anomalies in $(c/a)(P)$ will be analyzed subsequently. Before, we check the dependence of c/a on the volume in detail, which looks linear at first glance.

We performed linear fits to the individual data sets in the volume range $0.87 < V/V_0 < 1$, accounting for

	χ_n	σ	$V_0/\text{\AA}^3$
experiment (Occelli <i>et al.</i>) ¹¹	0.73	$7.4 \cdot 10^{-5}$	27.949
experiment (Takemura) ¹²	1.22	$1.2 \cdot 10^{-4}$	27.977
present calculation		$5.9 \cdot 10^{-5}$	27.87
calculation by Ma <i>et al.</i> ¹⁴		$8.1 \cdot 10^{-5}$	28.48

TABLE I: Quality of linear fits to the $(c/a)(V/V_0)$ data displayed in Figure 8, upper panel, in the range $0.87 < V/V_0 < 1$. For the definition of χ_n and σ see text. The fourth column displays the values used for V_0 . Values of adjustable parameters are given in the Appendix.

the known uncertainties of the experimental values, and considering the theoretical data points with equal weight. To characterize the quality of the fits, Table I displays $\chi_n = \sqrt{\chi^2/(n_p - n_e)}$ where χ^2 denotes the sum of the error weighted square deviations, n_p the number of the data points, and n_e the number of adjustable parameters, here 2. Moreover, for all data sets, Table I gives estimates of the standard deviation σ presuming validity of the linear dependence and uniform uncertainties of all data points included. Two conclusions can be drawn from this check: (i) the dependence of c/a on volume is linear within experimental accuracy according to the χ_n values, and (ii) the random errors of the theoretical data are comparable with the experimental inaccuracy. A linear fit of our calculation results for the whole volume range, $0.78 < V/V_0 < 1$, yields a σ value of $8.7 \cdot 10^{-5}$, resulting from a slight non-linearity at higher compressions.

Now we come to the key question of a possible anomaly in $(c/a)(P)$ at about 25 GPa, green (gray) dashed-dotted line in the lower panel of Figure 8. We stress again, in accordance with Refs. 11 and 14, that there is no doubt about the linearity of $(c/a)(V/V_0)$ within experimental precision. Thus, if $(c/a)(P)$ would be piecewise linear, as suggested by Occelli *et al.*, Sahu and Kleinman, as well as Ma *et al.*, then $P(V/V_0)$ had to be piecewise linear as well. In turn, this would imply a zero pressure derivative of the bulk modulus, $B' = 0$, in each of the pressure regions below and above the anomaly - a clear contradiction with the EOS fits by Occelli *et al.* who find $B' \approx 4$ in both regions.¹¹

Given a non-zero pressure derivative of the bulk modulus, $P(V)$ could most simply be approximated by a second-order polynomial. Since c/a is linear in the volume, this approximation translates into a square-root dependence of c/a on pressure:

$$(c/a)(P) = (c/a)_m + d\sqrt{(P + P_m)}, \quad (2)$$

where $(c/a)_m$, d , and P_m are fit parameters.

It is clear, that a square-root behavior can be fitted by two linear pieces within a restricted range. Table II gives a comparison of square-root and piece-wise linear fits between zero and 60 GPa, which is the range covered by all of the data sets. (We do not take into account the data by Sahu and Kleinman, since they have only four

	Eq. (2)		piece-wise linear function			
			kink: 25 GPa		kink: 27 GPa	
	χ_n	σ	χ_n	σ	χ_n	σ
exp. (Occelli <i>et al.</i>) ¹¹	0.69	$6.8 \cdot 10^{-5}$	0.71	$7.4 \cdot 10^{-5}$	0.85	$8.5 \cdot 10^{-5}$
exp. (Takemura) ¹²	1.27	$1.3 \cdot 10^{-4}$	1.28	$1.3 \cdot 10^{-4}$	1.26	$1.3 \cdot 10^{-4}$
present calculation		$7.5 \cdot 10^{-5}$		$1.1 \cdot 10^{-4}$		$1.0 \cdot 10^{-4}$
calc. by Ma <i>et al.</i> ¹⁴		$7.8 \cdot 10^{-5}$		$1.0 \cdot 10^{-4}$		$9.7 \cdot 10^{-5}$

TABLE II: Quality of different fits to the data displayed in Figure 8, lower panel, in the pressure range between zero and 60 GPa. For the definition of χ_n and σ see text. Values of adjustable parameters are given in the Appendix.

points in the considered pressure range.) According to Refs. 11 and 14 we assumed the kink between the linear pieces at the suggested 25 GPa and 27 GPa, respectively.

Table II shows that both kinds of fits work almost equally well, with a small advantage of the square-root fit. Additionally for the data by Occelli *et al.*, we performed a four parameter piece-wise linear fit, allowing the critical pressure P_c to vary: Only a slightly better approximation was obtained ($\chi_n = 0.51$ for the complete data set), but P_c amounts to 19 ± 2 GPa. Finally we have checked parabolic and cubic fits, which yield very similar χ_n and σ values compared to the square-root fit.

According to Tab. II and the non-vanishing pressure derivative of the compressibility argument above, we believe that there is not enough evidence to conclude an anomaly at about 25 GPa. Regarding the DFT calculations, no peculiarity in the band structure or Fermi surface topology is observed in this pressure range. Thus, it would be artificial to expect an anomaly in the computed elastic data. Of course, regarding the experiments, other than electronic origins of an anomaly cannot be excluded. However, in our opinion, such an anomaly is not proved by in the available data sets. Error correlations mentioned in Ref. 11 could be caused by the change of the experimental setup at 26 GPa.

VII. SUMMARY

We predict three Lifshitz transitions to occur in hexagonal close-packed Osmium under pressure up to 180 GPa. The corresponding van Hove singularities in the density of states are probably too small to produce any measurable effect in the elastic properties but may be detectable in transport properties. Since the lowest critical pressure amounts to 70...80 GPa, it is not related with a previously suggested kink at 25 GPa in the pressure dependence of c/a . We demonstrate that this kink can be replaced by a smooth dependence without any change in the statistic significance. Thus, we cannot confirm the electronic origin of the proposed anomaly.

Acknowledgments

We are indebted to Ulrike Nitzsche, Ingo Opahle, Norbert Mattern, and Ulrich Schwarz for enlightening discussions. Yanming Ma, Daniel L. Farber, B.R. Sahu, and Leonard Kleinman kindly provided numerical data from their related publications. Financial support by DFG, SPP 1145, is gratefully acknowledged.

APPENDIX

1. Linear fit to $(c/a)(V/V_0)$

$$c/a = A \cdot (V/V_0) + B$$

	A	B
exp. (Ocelli <i>et al.</i>) ¹¹	-0.0539(4)	1.6339(4)
exp. (Takemura) ¹²	-0.0540(6)	1.6339(6)
present calculation	-0.0594(2)	1.6445(1)
calc. by Ma <i>et al.</i> ¹⁴	-0.0678(6)	1.6450(6)

2. Square-root fit to $(c/a)(P)$

	$(c/a)_m$	$d/\text{GPa}^{-1/2}$	P_m/GPa
exp. (Ocelli <i>et al.</i>) ¹¹	1.572(1)	0.00146(9)	28(5)
exp. (Takemura) ¹²	1.572(2)	0.0015(1)	30(9)
present calculation	1.5753(8)	0.00162(5)	37(4)
calc. by Ma <i>et al.</i> ¹⁴	1.5708(10)	0.00157(8)	16(4)

3. Piece-wise linear fit to $(c/a)(P)$

a. Kink at 25 GPa

A - c/a at $P = 0$ GPa

B - slope between 0 GPa and 25 GPa

C - slope between 25 GPa and 60 GPa

	A	$10^4 B/\text{GPa}^{-1}$	$10^4 C/\text{GPa}^{-1}$
exp. (Ocelli <i>et al.</i>) ¹¹	1.579933(9)	1.23(2)	0.80(3)
exp. (Takemura) ¹²	1.57995(4)	1.17(3)	0.86(3)
present calculation	1.58525(2)	1.117(8)	0.955(6)
calc. by Ma <i>et al.</i> ¹⁴	1.57729(7)	1.46(3)	1.06(4)

b. Kink at 27 GPa

A - c/a at $P = 0$ GPa

B - slope between 0 GPa and 27 GPa

C - slope between 27 GPa and 60 GPa

	A	$10^4 B/\text{GPa}^{-1}$	$10^4 C/\text{GPa}^{-1}$
exp. (Ocelli <i>et al.</i>) ¹¹	1.579935(2)	1.219(14)	0.78(4)
exp. (Takemura) ¹²	1.57995(4)	1.16(3)	0.84(3)
present calculation	1.58525(2)	1.113(8)	0.940(7)
calc. by Ma <i>et al.</i> ¹⁴	1.57730(6)	1.45(3)	1.02(4)

¹ I. M. Lifshitz, Sov. Phys. JETP **11**, 1130 (1960).

² Y. M. Blanter, M. I. Kaganov, A. V. Pantsulaya, and A. A. Varlamov, Phys. Rep. **245**, 159 (1994).

³ A. A. Varlamov, V. S. Egorov, and A. V. Pantsulaya, Adv. Phys. **38**, 469 (1989).

⁴ N. Kozlova, J. Hagel, M. Doerr, J. Wosnitza, D. Eckert, K.-H. Müller, L. Schultz, I. Opahle, S. Elgazzar, M. Richter, G. Goll, H. von Lohneysen, G. Zwicknagl, T. Yoshino, and T. Takabatake, Phys. Rev. Lett. **95**, 086403 (2005).

⁵ B. K. Godwal, A. Jayaraman, S. Meenakshi, R. S. Rao, S. K. Sikka, and V. Vijayakumar, Phys. Rev. B **57**, 773 (1998).

⁶ H. Rosner, D. Koudela, U. Schwarz, A. Handstein, M. Hanfland, I. Opahle, K. Koepernik, M. Kuz'min, K.-H. Müller,

J. A. Mydosh, and M. Richter, Nature Physics **2**, 469 (2006).

⁷ Takemura Kenichi, Phys. Rev. B **56**, 5170 (1997).

⁸ Takemura Kenichi, Phys. Rev. B **60**, 6171 (1999).

⁹ G. Steinle-Neumann, L. Stixrude, and R. E. Cohen, Phys. Rev. B **63**, 054103 (2001).

¹⁰ A. B. Garg, V. Vijayakumar, P. Modak, D. M. Gaitonde, R. S. Rao, B. K. Godwal, and S. K. Sikka, J. Phys.: Condens. Matter **14**, 8795 (2002).

¹¹ F. Ocelli, D. L. Farber, J. Badro, C. M. Aracne, D. M. Teter, M. Hanfland, B. Canny, and B. Couzinet, Phys. Rev. Lett. **93**, 095502 (2004).

¹² Takemura Kenichi, Phys. Rev. B **70**, 012101 (2004).

¹³ B. R. Sahu and L. Kleinman, Phys. Rev. B **72**, 113106

- (2005).
- ¹⁴ Y. M. Ma, T. Cui, L. J. Zhang, Y. Xie, G. T. Zou, J. S. Tse, X. Gao, and D. D. Klug, Phys. Rev. B **72**, 174103 (2005).
 - ¹⁵ K. Koepernik and H. Eschrig, Phys. Rev. B **59**, 1743 (1999), <http://www.flo.de>.
 - ¹⁶ M. M. Hebbache, Int. J. Refract. Met. Hard Mat. **24**, 6 (2006).
 - ¹⁷ G. Lehmann and M. Taut, Phys. Status Solidi B **54**, 469 (1972).
 - ¹⁸ J. P. Perdew and Y. Wang, Phys. Rev. B **45**, 13244 (1992).
 - ¹⁹ H. Eschrig, M. Richter, and I. Opahle, in *Relativistic Electronic Structure Theory - Part II: Applications*, edited by P. Schwerdtfeger (Elsevier, Amsterdam, 2004), pp. 723–776.
 - ²⁰ G. N. Kamm and J. R. Anderson, Phys. Rev. B **2**, 2944 (1970).
 - ²¹ V. I. Smelyansky, A. Y. Perlov, and V. N. Antonov, J. Phys.: Condens. Matter **2**, 9373 (1990).

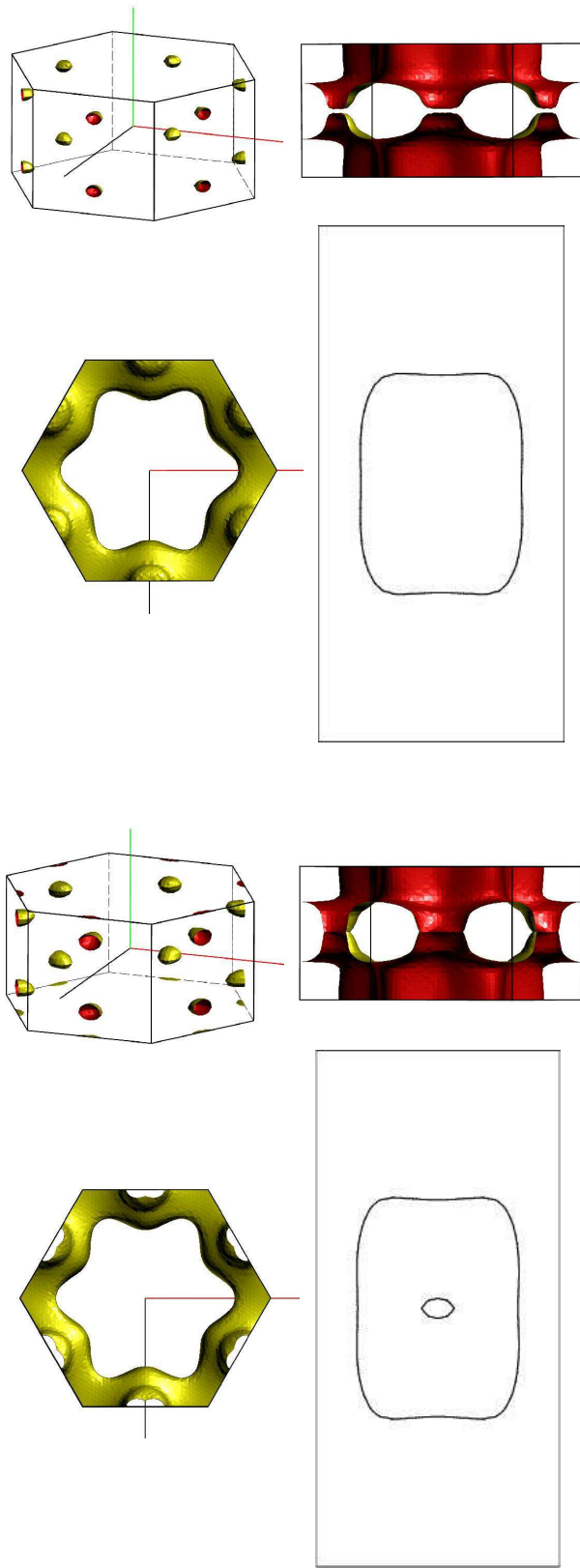


FIG. 3: (color online). Comparison between the Fermi surface of Osmium at zero pressure ($V = 27.87 \text{ \AA}^3$ first row) and under high pressure (second row, $P \approx 180 \text{ GPa}$, $V = 22.00 \text{ \AA}^3$). The upper left panels show the first FS sheet, the upper right and the lower left panels show the second FS sheet in a side view and in a top view, respectively. In order to make the connectivity better visible, the side view is shifted in z -direction, such that the BZ edge lies in the middle of the picture. The lower right panels display a cut through the fourth sheet of the Fermi surface in the y - z plane. Colors are explained in Figure 2.

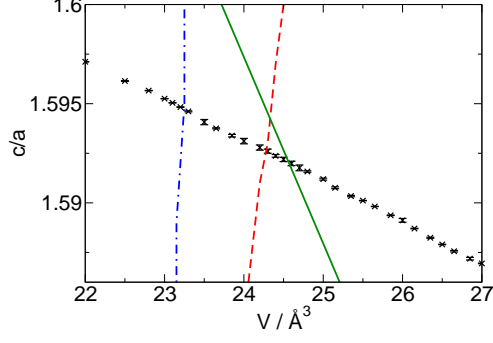


FIG. 4: (color online). Dependence of the FS topology on volume and c/a . Black symbols with error bars: calculated relaxed c/a versus unit cell volume. Green (gray) full line: ETT at the Γ -point. Red (gray) dashed line: ETT at the symmetry-line LH. Blue (black) dash-dotted line: ETT at the L-point.

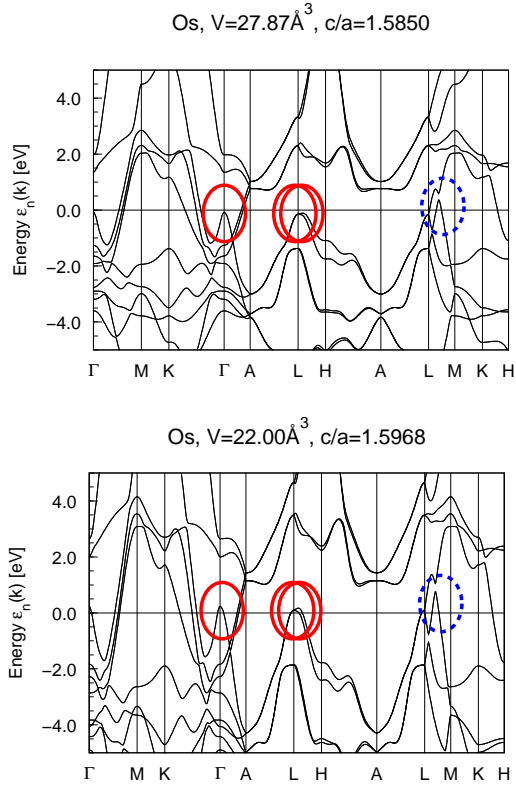


FIG. 5: (color online). Band structure of Osmium. Upper panel: zero pressure; lower panel: $P \approx 180$ GPa. The red (gray) circles (full lines) mark points in \mathbf{k} -space where a band maximum crosses the Fermi level under pressure. The blue (black) circle (dashed lines) marks the location of an ETT proposed by Occelli *et al.*¹¹

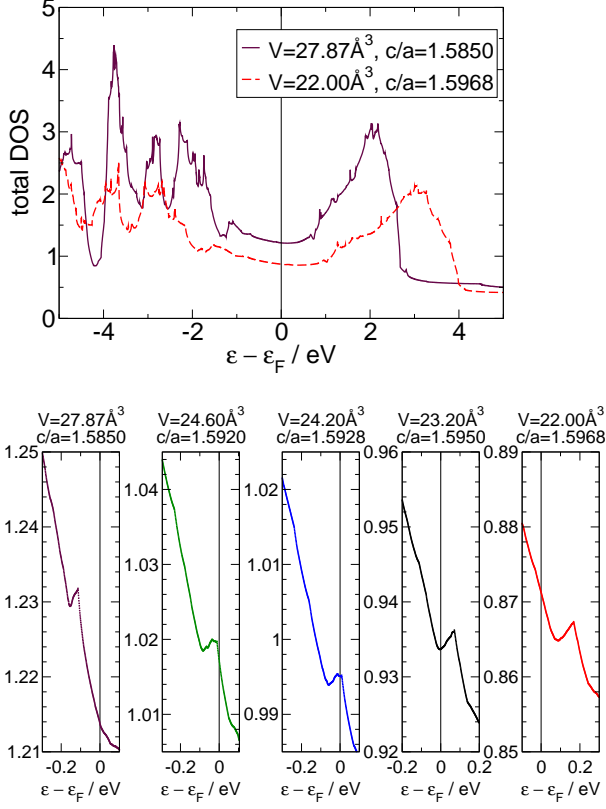


FIG. 6: (color online). Upper panel: Total density of states of Osmium at two different volumes. Maroon (black) full lines: zero pressure; red (light-gray) dashed lines: pressure of about 180 GPa. The Fermi level is situated in a smooth valley of the DOS. Five lower panels, from left to right: magnification of the DOS around the Fermi level at zero pressure; at that pressure, where the ellipsoid at the Γ -point appears, at that pressure, where the neck is created, at that pressure, where the ellipsoid at the L-point appears, and at a pressure of about 180 GPa.

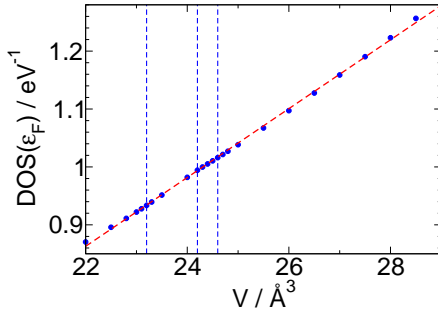


FIG. 7: (color online). DOS at the Fermi energy versus volume. The red (gray) solid line shows a linear function fitted to the data. The blue (black) dashed lines mark those volumes, where the Lifshitz transitions take place.

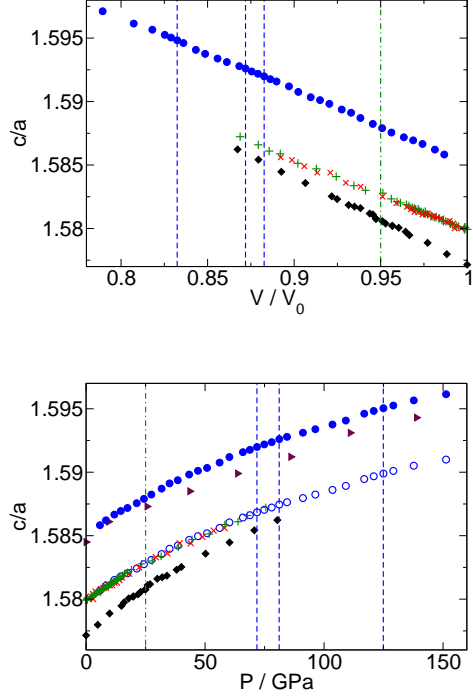


FIG. 8: (color online). Upper panel: relaxed c/a -ratio against normalized volume; lower panel: relaxed c/a -ratio against pressure. The meaning of the symbols $+$, \times , \bullet and green (gray) dashed-dotted line is the same as in Figure 1, lower panel. Moreover, black diamonds denote calculations by Ma *et al.*¹⁴ Additional data from calculations by Sahu and Kleinman are denoted by violet (black) triangles in the lower panel.¹³ The blue (black) open circles are a shift of our data down by 0.00515. Error-bars are below symbol size. The position of the Lifshitz transitions (blue (black) lines) in the lower graph was obtained from the FPLO EOS.